Spin-Orbit Coupling and Anisotropy of Spin Splitting in Quantum Dots

J. Könemann,[1] R. J. Haug,[1] D. K. Maude,[2] V. I. Fal'ko,[3,4] and B. L. Altshuler[4,5]

[1]*Institut für Festkörperphysik, Universität Hannover, Appelstrasse 2, D-30167 Hannover, Germany*
[2]*High Magnetic Field Laboratory, CNRS, 25 Avenue des Martyrs, BP 166, F-38042 Grenoble cedex 9, France*
[3]*Physics Department, Lancaster University, Lancaster LA1 4YB, United Kingdom*
[4]*Physics Department, Jadwin Hall, Princeton University, New Jersey 08450, USA*
[5]*NEC Laboratories America, Inc., 4 Independence Way, Princeton, New Jersey 08540, USA*

(Received 3 September 2004; published 7 June 2005)

In lateral quantum dots, the combined effect of both Dresselhaus and Bychkov-Rashba spin-orbit coupling is equivalent to an effective magnetic field $\pm B_{\mathrm{SO}}$ which has the opposite sign for $s_z = \pm 1/2$ spin electrons. When the external magnetic field is perpendicular to the planar structure, the field B_{SO} generates an additional splitting for electron states as compared to the spin splitting in the in-plane field orientation. The anisotropy of spin splitting has been measured and then analyzed in terms of spin-orbit coupling in several AlGaAs/GaAs quantum dots by means of resonant tunneling spectroscopy. From the measured values and sign of the anisotropy we are able to determine the dominating spin-orbit coupling mechanism.

DOI: 10.1103/PhysRevLett.94.226404 PACS numbers: 71.70.Ej, 72.25.−b, 73.23.−b, 85.75.−d

A better understanding of the spin-orbit (SO) effects is crucial for the implementation of the coherent manipulation of the electron spin [1,2] in quantum dots and wires. SO coupling in III-V semiconductor structures is usually composed of two interplaying contributions of different symmetries,

$$\mathcal{H}_{\mathrm{SO}} = \varrho_{\mathrm{D}}(p_x s_x - p_y s_y) + \varrho_{\mathrm{BR}}(p_y s_x - p_x s_y). \quad (1)$$

The first term is reminiscent of the Dresselhaus SO coupling in zinc blende bulk semiconductors [3,4] (it reflects the inversion asymmetry of GaAs). The second term in Eq. (1) is the interface-induced coupling of the Bychkov-Rashba type [5]. It is difficult to separate the effects of the two SO coupling mechanisms in quantum transport measurements and spin relaxation [6–11] (except for optical experiments [12,13]), and even to determine which one is dominant. At the same time coherent spin manipulation as well as the spin-Hall effect [2,14,15] depend on the balance between the two mechanisms.

Here, we show that the relative strength of the Dresselhaus and Bychkov-Rashba SO coupling mechanisms in a device can be determined from the anisotropy of the spin splitting. We exploit single-electron resonant tunneling spectroscopy [16] to observe the difference $\Delta_\perp - \Delta_\parallel$ in spin splitting in a double-barrier structure subjected to a magnetic field perpendicular ($\Delta_\perp$) and parallel ($\Delta_\parallel$) to the plane of the quantum well. We analyze this anisotropy within the framework of the theory of SO coupling in lateral quantum dots [8,9]. It is shown below that the two mechanisms cause anisotropy of opposite signs, and that

$$\Delta_\perp - \Delta_\parallel \propto (-g/|g|)(\varrho_{\mathrm{BR}}^2 - \varrho_{\mathrm{D}}^2), \quad (2)$$

where g is the quantum well electron Lande g factor in the in-plane magnetic field.

The experiment was performed with two highly asymmetric double-barrier resonant tunneling devices with an undoped 10 nm wide GaAs quantum well being sandwiched between 5 and 8 nm thick $Al_{0.3}Ga_{0.7}As$ tunneling barriers separated from the highly doped GaAs contacts (Si doped with $n_S = 4 \times 10^{17}$ cm^{-3}) by 7 nm thick undoped GaAs spacer layers. The samples were fabricated as pillars of 2 μm (sample A) and 40 μm diameter (sample B). dc measurements of the I-V characteristics were performed in a dilution refrigerator at 20 mK base temperature for two different orientations of the magnetic field, see Fig. 1(a). The studied GaAs quantum well embedded between two AlGaAs barriers can be viewed as a two-dimensional system with the edges and residual impurities confining the lateral electron motion and thus forming dots. Tunneling through the lowest state of the dot, at the energy E_0 and with lateral extent λ, produces the lowest resonance peak in the differential conductance, whereas its excited states are responsible for additional peaks in dI/dV, which all move in a magnetic field B_z perpendicular to the quantum well, as shown in Figs. 2 and 3 . The magnetic field dependence of energy levels can be illustrated using the model of parabolic confinement, $V(\mathbf{r}) = \frac{1}{2}m\omega^2\mathbf{r}^2$, with the extension of the wave function $\lambda \sim \sqrt{\hbar/\omega m}$, where the

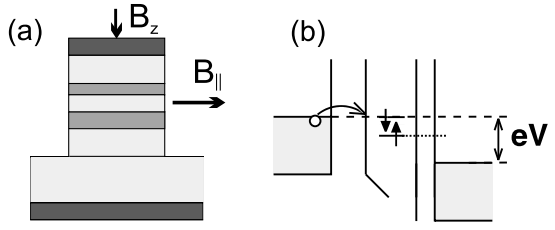

FIG. 1. Schematic picture (a) and energy diagram (b) of the studied device under finite bias and finite magnetic field.

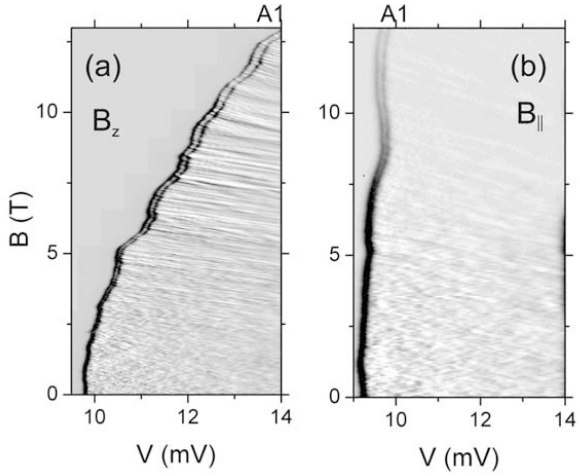

FIG. 2. Differential conductance as a gray-scale plot for sample A ($\hbar\omega = 31.2$ meV) as a function of bias voltage and magnetic field for (a) B_z being perpendicular to the quantum well plane, and (b) $B_\parallel$, $T = 20$ mK.

spectrum of quantum dot states $|n_+ n_-\rangle$, $n_\pm = 0, 1, 2, \ldots$ is described by

$$E_{n_+ n_-} = E_0 + \hbar\sqrt{\omega^2 + (\omega_c/2)^2} - \hbar\omega + \sum_{\pm} n_\pm \hbar\omega_\pm \qquad (3)$$

$$\omega_\pm = \sqrt{\omega^2 + (\omega_c/2)^2} \pm \tfrac{1}{2}\omega_c, \qquad \omega_c = eB/m.$$

For a strongly bound state or at low fields, such that $\omega > \omega_c$ (also $\lambda < \lambda_B$, where $\lambda_B = \sqrt{\hbar/eB_z}$), the first tunneling resonance experiences a diamagnetic shift $E_{00} \approx E_0 + \hbar\omega_c^2/8\omega$, which is quadratic in B_z. For $\omega \ll \omega_c$ at high fields, $\omega_+ \approx \omega_c$ and $\omega_- \approx \omega^2/\omega_c \ll \omega_c$, the diamagnetic shift of several low-energy states in a dot follows approximately the energy of the lowest 2D Landau level, $E_{0n_-} \approx [E_0 - \hbar\omega + (n_- + 1)\hbar\omega^2/\omega_c] + 1/2\hbar\omega_c(B_z)$. In the structures studied, both weakly and strongly bound states have been seen.

Figure 2(a) shows the differential conductance peak $A1$ found in sample A and attributed to a strongly bound state ($\hbar\omega = 31.2$ meV extracted from the diamagnetic shift using an energy-voltage conversion factor of $\alpha = 0.5$ [17]), presumably formed by a growth-induced local potential minimum. Several differential conductance peaks, $B1$–$B4$ and BX, were observed in sample B. The magnetic field dependence of their positions shown in Fig. 3(a) complies with the magnetospectrum in a parabolic potential with $\hbar\omega = 13.8$ meV [18]. We attribute the large voltage onset of around 240 mV in sample B to strong serial resistances due to partly compensated regions in emitter and collector [19]. The data shown in Fig. 2(b) and 3(b) taken on the same structures subjected to an in-plane magnetic field do not display a diamagnetic shift and confirm the 2D nature of the dots.

In both magnetic field directions, all peaks in dI/dV resolve into two at high enough field values, manifesting the spin splitting of each dot state. Spin splittings extracted from the data shown in Figs. 2 and 3 are gathered in Fig. 4: (a) shows the data for sample A averaged over a field

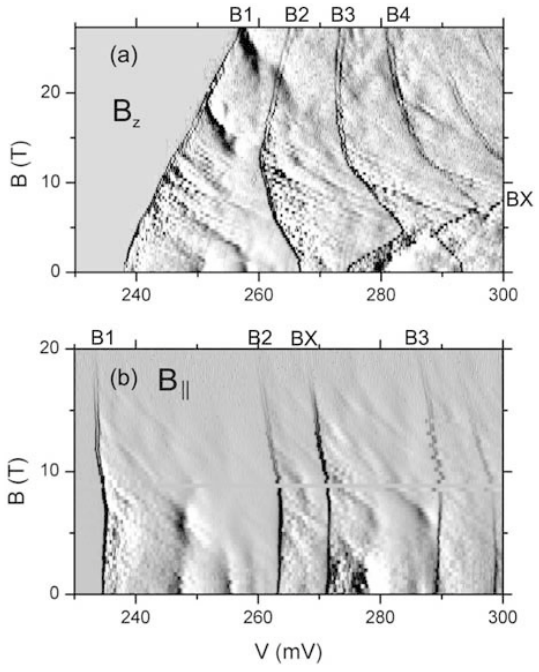

FIG. 3. Differential conductance as a gray-scale plot for sample B ($\hbar\omega = 13.8$ meV) as a function of bias voltage and magnetic field for (a) B_z being perpendicular to the quantum well plane, and (b) $B_\parallel$, $T = 20$ mK.

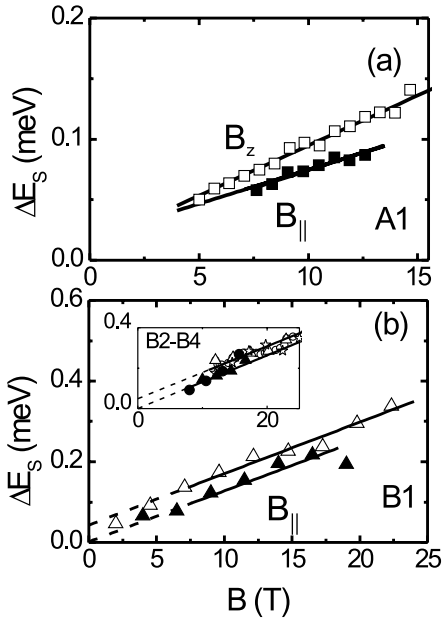

FIG. 4. (a) Spin splitting of the state $A1$ of sample A for both B-field configurations. (b) Spin splitting of the state $B1$ of sample B for both B-field configurations. Solid lines represent the result of a linear fit to the high-field part of the data. Inset shows the spin splitting of the states $B2$ (triangles), $B3$ (circles), and $B4$ (stars) for both B-field configurations.

interval of 0.33 T, whereas (b) shows the field dependence of splittings in sample B averaged over an interval of 3 T to eliminate the influence of fluctuations of the local density of states of the emitter [20]. In Fig. 4 a distinct anisotropy of the peak splitting is displayed, with the splitting caused by the out-of-plane field (open symbols) being systematically larger than what is created by the in-plane field (closed symbols).

The observed values of spin splitting anisotropy are much larger and have the opposite sign to what might be expected from the kinetic energy dependence, $g = -0.44 + E(dg/dE)$ of the electron g factor across the conduction band in GaAs. Using $dg/dE \sim +2\ \mathrm{eV}^{-1}$ [21], we estimate that the diamagnetic shift (which increases the electron kinetic energy in a perpendicular magnetic field) would further reduce the value of g at higher fields by $(\hbar\omega_c/2)(dg/dE)$. The latter is less than the observed anisotropy in the peak $B1$. One may also notice that the anisotropy of spin splitting of the excited dot states $B2$–$B4$ shown in the inset to Fig. 4 is the same as of $B1$, despite a larger kinetic energy of an electron in them.

Although one may address the interpretation of this observation using a microscopic model of the quantum well based upon $\mathbf{kp}$ theory, such as developed in Refs. [22], below we adopt an alternative phenomenological approach describing the SO coupling in a quantum well using the effective Hamiltonian in Eq. (1). This enables us to express the spin splitting anisotropy of the electron in a lateral quantum dot in terms of the effective magnetic field $B_{\mathrm{SO}} = (\hbar m^2)/(2e)(\varrho_{\mathrm{BR}}^2 - \varrho_{\mathrm{D}}^2)$ recently discussed in relation to the geometrical Berry phase in quantum dots [8,9] and rings [23].

For a quantum well lying in the (001) crystallographic plane of GaAs it is convenient to choose coordinates along crystallographic directions $\hat{\mathbf{e}}_1 = [110]$ and $\hat{\mathbf{e}}_2 = [\bar{1}10]$, and to study the effective 2D Hamiltonian in the form

$$\mathcal{H} = \frac{(-i\hbar\nabla - \mathbf{A} - \mathbf{a})^2}{2m} + \frac{g\epsilon_{\mathrm{Z}}}{|g|2}\mathbf{l}\sigma + \mathrm{V}(\mathbf{r}), \qquad (4)$$

$$\mathbf{a} = \frac{\hbar\sigma_2\hat{\mathbf{e}}_1}{2\lambda_1} - \frac{\hbar\sigma_1\hat{\mathbf{e}}_2}{2\lambda_2}, \qquad (5)$$

where $\mathbf{A} = \frac{e}{2}B_z[\mathbf{r}\times\hat{\mathbf{e}}_z]$, $\mathbf{l} = \mathbf{B}/B$, $\sigma = (\sigma_1, \sigma_2, \sigma_3)$ is the vector of Pauli matrices, and $\epsilon_{\mathrm{Z}} = |g\mu_{\mathrm{B}}B|$ is the Zeeman energy (in a 10 nm wide GaAs/AlGaAs quantum well, $g < 0$ according to Snelling *et al.* [21]; and in the above expressions, we have already taken into account the negative sign of the electron charge, so that $e > 0$). The parameters ϱ_{D} and ϱ_{BR} of the SO coupling defined in Eq. (1) for a conventional choice of axes, $\hat{\mathbf{x}} = [100]$ and $\hat{\mathbf{y}} = [010]$, appear in the uniform non-Abelian vector potential $\mathbf{a}$ in Eq. (4) via the inverse of the SO coupling length $\lambda_{1(2)}$ as $\lambda_1^{-1} = (\varrho_{\mathrm{D}} - \varrho_{\mathrm{BR}})m$ and $\lambda_2^{-1} = -(\varrho_{\mathrm{BR}} + \varrho_{\mathrm{D}})m$, where $2\pi\lambda_{1(2)}$ characterizes the distance at which spin precession of a polarized electron moving along crystallographic direction $\hat{\mathbf{e}}_{1(2)}$ undergoes one complete revolution.

To analyze the case of a weak SO coupling for electrons bound in a quantum dot, $\lambda_{1,2} \gg \lambda$, we follow Refs. [8,9] and perform a nonuniform unitary transformation to the electron wave function, $\psi(\mathbf{r}) = U(\mathbf{r})\tilde{\psi}(\mathbf{r})$ and the Hamiltonian in Eq. (4),

$$U = \exp\{\tfrac{i}{2}[\lambda_1^{-1}x_1\sigma_2 - \lambda_2^{-1}x_2\sigma_1]\}, \qquad \tilde{\mathcal{H}} = U^\dagger\mathcal{H}U.$$

This transformation rotates locally the spin space by the angle $R = \sqrt{(x_1/\lambda_1)^2 + (x_2/\lambda_2)^2}$ around the unit vector $\hat{\mathbf{n}} = (\lambda_1^{-1}x_1\hat{\mathbf{e}}_2 - \lambda_2^{-1}x_2\hat{\mathbf{e}}_1)/R$. As a result, the coordinate frame for the electron spin set in the center of the dot, $x_{1,2} = 0$, gets adjusted to the local orientation determined by the SO-induced spin precession upon its displacement along the radius vector $\mathbf{r}$. The energy spectrum can be found from the transformed Hamiltonian

$$\tilde{\mathcal{H}} = \frac{1}{2m}(-i\hbar\nabla - \mathbf{A} - \tilde{\mathbf{a}})^2 + \tfrac{1}{2}\epsilon_{\mathrm{Z}}\tilde{\mathbf{l}}\sigma + V(\mathbf{r}),$$

where $\tilde{\mathbf{a}} = U^\dagger\mathbf{a}U + i\hbar U^\dagger\nabla U$ and $\tilde{\mathbf{l}}(\mathbf{r}) = (\mathbf{l}\cdot\hat{\mathbf{n}})\hat{\mathbf{n}} + \hat{\mathbf{n}}\times[\mathbf{l}\times\hat{\mathbf{n}}]\cos R - [\mathbf{l}\times\hat{\mathbf{n}}]\sin R$. The transformation $U(\mathbf{r})$ aims to gauge out [8,9,24,25] spin-orbit coupling, which appears in Eq. (4) in the form of uniform spin-dependent vector potential in Eq. (5). The latter goal cannot be achieved in full, since Pauli matrices do not commute with each other. However, for a weak SO coupling [$\lambda_{1,2} \gg \lambda$] and small rotation angles $R \ll 1$, the residual $\tilde{\mathbf{a}}$, [9]

$$\tilde{\mathbf{a}} = -\frac{[\mathbf{r}\times\hat{\mathbf{e}}_3]}{4\lambda_1\lambda_2}\hbar\sigma_3 + \hbar\lambda_{1,2}^{-1}\mathcal{O}[R^2], \qquad (6)$$

is dominated by the "vector potential" of an effective magnetic field which has the opposite sign for spin "up" and "down" electrons in the quantum dot, [8,9]

$$B_{\mathrm{eff}} = B_z - \sigma_3 B_{\mathrm{SO}}. \qquad (7)$$

It is this difference in the effective magnetic field seen by an electron in the adjusted spin frame that causes the spin splitting anisotropy. For the in-plane magnetic field orientation ($B_z = 0$), the effective field $B_{\mathrm{eff}} = \pm B_{\mathrm{SO}}$ produces the same negligibly small "diamagnetic" shift $\sim B_{\mathrm{SO}}^2$ in the orbital motion energy of both spin components. Accordingly it does not alter the value of the quantum well Zeeman splitting, $\Delta_\parallel = \epsilon_{\mathrm{Z}}$.

For the perpendicular magnetic field orientation ($\mathbf{B} = B\hat{\mathbf{e}}_z$), the difference in $B_{\mathrm{eff}} = B_z \pm B_{\mathrm{SO}}$ generates the difference in the effective diamagnetic shift for two spin states and, therefore, an additional energy splitting. It results in the anisotropy of spin splitting in the lowest quantum dot state

$$\Delta_\perp - \Delta_\parallel = \frac{-gdE_{00}}{|g|dBz}2B_{\mathrm{SO}} = \frac{-g\frac{\omega_c e\hbar}{2m}B_{\mathrm{SO}}}{|g|\sqrt{\omega^2 + (\frac{1}{2}\omega_c)^2}}. \qquad (8)$$

Equation (8) is valid in both low and high magnetic field regimes. Its low-field asymptotic

$$\Delta_\perp - \Delta_\parallel \approx \left(\frac{-g}{|g|}\right)B\hbar e^2 B_{\mathrm{SO}}/(2\omega m^2) \qquad (9)$$

TABLE I. Experimental parameters of the spin-orbit characteristics for sample A and B, as discussed in the text.

samples	A	B	
peak	$A1$	$B1$	$B2$–$B4$
$\frac{e\hbar}{m}B_{\mathrm{SO}}$	32 ± 2 μeV	43 ± 10 μeV	44 ± 16 μeV
B_{SO}	19 mT	25 mT	

for $\omega_c < \omega$ also describes the situation of a strongly bound electron, such as the resonance level $A1$. The high-field asymptotic of the result in Eq. (8),

$$\Delta_\perp - \Delta_\parallel \approx \left(\frac{-g}{|g|}\right)\frac{e\hbar}{m}B_{\mathrm{SO}} \quad \text{for } \omega_c \gg \omega, \tag{10}$$

simultaneously describes the anisotropy of the spin splitting of the few lowest quantum dot states E_{0n_-}. The anisotropy energy transforms into an offset with the sign dependent on the sign of $B_{\mathrm{SO}} \propto (\varrho_{\mathrm{BR}}^2 - \varrho_{\mathrm{D}}^2)$ in Eq. (7) and on the sign of the electron g factor. Finally, we apply Eqs. (8)–(10) to analyze the peak splitting data shown in Fig. 4. Since in a 10 nm wide GaAs quantum well the bare value of the g factor is negative [21], larger values of spin splitting in a perpendicular field mean that $B_{\mathrm{SO}} \propto (\varrho_{\mathrm{BR}}^2 - \varrho_{\mathrm{D}}^2) > 0$, pointing at the dominance of the Bychkov-Rashba term in the SO coupling, presumably, due to the electron penetrating into the AlGaAs barrier which is enhanced in a narrow quantum well.

The fit to the experimentally observed anisotropy produces values of $(e\hbar/m)B_{\mathrm{SO}}$ which are shown in Table I and determine the effective field B_{SO} in each sample. $B_{\mathrm{SO}} = 25 \pm 6$ mT was obtained using Eq. (10) for $B1$ and agrees well with the value of 25 ± 8 mT for linear fitting of $B2$–$B4$. The strongly confined state observed in sample A [peak $A1$, Fig. 4(a)] was analyzed using Eq. (9), and we extracted $B_{\mathrm{SO}} = 19 \pm 1$ mT. The sign of SO coupling characteristics in $B_{\mathrm{SO}} \propto (\varrho_{\mathrm{BR}}^2 - \varrho_{\mathrm{D}}^2)$ suggests that in a narrow quantum well Bychkov-Rashba coupling is dominant—in contrast to wide quantum wells investigated in Raman scattering [12]. The extracted SO coupling is also stronger than that estimated from the bulk Dresselhaus term, $2\gamma\hbar^{-4}\sum_{ijk}\epsilon^{ijk}p_i^2 p_j s_j$, (where ϵ^{ijk} is the antisymmetric tensor) using $\gamma = (26 \pm 5)$ eVÅ^3 collected from Refs. [7,12]. For the quantum well width $w = 10$ nm, the Dresselhaus mechanism alone would generate B_{SO}, which reduces the Zeeman splitting and is of much smaller absolute value, $(\hbar^2 m/2)\varrho_{\mathrm{D}}^2 \approx 2\pi^4 m(\gamma/w^2)^2 \approx 12$ μeV. Using this estimate, we can deduce the strength of the Bychkov-Rashba coupling in quantum wells in the samples $B(A)$ as, at least, $(\hbar^2 m/2)\varrho_{\mathrm{BR}}^2 \sim 54(44)$ μeV.

We acknowledge sample growth by A. Förster, H. Lüth, V. Avrutin, and A. Waag. This work was partially supported by BMBF (R. H.), DFG (R. H.), by EPSRC (V. F.), DARPA under the QuIST Program (B. A.), and by ARDA/ARO Quantum Computing Program (B. A.).

[1] J. M. Elzerman *et al.*, Phys. Rev. B **67**, 161308 (2003); R. Hanson *et al.*, Phys. Rev. Lett. **91**, 196802 (2003)
[2] D. Loss and D. P. DiVincenzo, Phys. Rev. A **57**, 120 (1998); G. Burkard and D. Loss, Phys. Rev. Lett. **88**, 047903 (2002); D. Stepanenko *et al.*, Phys. Rev. B **68**, 115306 (2003).
[3] G. Dresselhaus, Phys. Rev. **100**, 580 (1955).
[4] F. Malcher, G. Lommer, and U. Rössler, Superlattices Microstruct. **2**, 267 (1986).
[5] Yu. Bychkov and E. Rashba, JETP Lett. **39**, 78 (1984); L. Wissinger *et al.*, Phys. Rev. B **58**, 15 375 (1998).
[6] F. Malcher, G. Lommer, and U. Rössler, Phys. Rev. Lett. **60**, 728 (1988).
[7] J. B. Miller *et al.*, Phys. Rev. Lett. **90**, 076807 (2003); W. Knap *et al.*, Phys. Rev. B **53**, 3912 (1996).
[8] I. L. Aleiner and V. I. Fal'ko, Phys. Rev. Lett. **87**, 256801 (2001).
[9] J.-H. Cremers, P. W. Brouwer, and V. I. Fal'ko, Phys. Rev. B **68**, 125329 (2003).
[10] D. M. Zumbühl *et al.*, Phys. Rev. Lett. **89**, 276803 (2002); J. A. Folk *et al.*, Phys. Rev. Lett. **86**, 2102 (2001).
[11] J. P. Lu *et al.*, Phys. Rev. Lett. **81**, 1282 (1998).
[12] B. Jusserand *et al.*, Phys. Rev. Lett. **69**, 848 (1992); D. Richards *et al.*, Phys. Rev. B **47**, 16 028 (1993); B. Jusserand *et al.*, Phys. Rev. B **51**, 4707 (1995).
[13] S. D. Ganichev *et al.*, Phys. Rev. Lett. **92**, 256601 (2004).
[14] E. I. Rashba and Al. L. Efros, Phys. Rev. Lett. **91**, 126405 (2003).
[15] J. Schliemann and D. Loss, Phys. Rev. B **68**, 165311 (2003).
[16] M. R. Deshpande *et al.*, *Proceedings of the ICPS-23* (World Scientific, Singapore, 1996) p. 1577; M. R. Deshpande *et al.*, Phys. Rev. Lett. **76**, 1328 (1996); A. S. G. Thornton *et al.*, Appl. Phys. Lett. **73**, 354 (1998); J. Könemann, P. König, and R. J. Haug, Physica E (Amsterdam) **13**, 675 (2002).
[17] P. König *et al.*, *Proceedings of the ICPS-25* (Springer, Berlin, 2000), p. 833.
[18] E. Räsänen *et al.*, Phys. Rev. B **70**, 115308 (2004).
[19] The partly compensated regions could be related to an unintentional doping with Mn acceptors, residual in the MBE of sample B.
[20] P. König, T. Schmidt, and R. J. Haug, Europhys. Lett. **54**, 495 (2001).
[21] M. J. Snelling *et al.*, Phys. Rev. B **45**, 3922 (1992); M. J. Snelling *et al.*, Phys. Rev. B **44**, 11 345 (1991); R. M. Hannak *et al.*, Solid State Commun. **93**, 313 (1995).
[22] A. Kiselev, E. Ivchenko, and U. Rössler, Phys. Rev. B **58**, 16 353 (1998); E. Ivchenko and A. Kiselev, Sov. Phys. Semicond. **26**, 827 (1992).
[23] A. F. Morpurgo *et al.*, Phys. Rev. Lett. **80**, 1050 (1998); F. E. Meijer *et al.*, Phys. Rev. B **70**, 201307 (2004).
[24] Y. Meir, Y. Gefen, and O. Entin-Wohlman, Phys. Rev. Lett. **63**, 798 (1989).
[25] H. Mathur and A. D. Stone, Phys. Rev. Lett. **68**, 2964 (1992); Y. Oreg and O. Entin-Wohlman Phys. Rev. B **46**, 2393 (1992); A. G. Aronov and Yu. B. Lyanda-Geller, Phys. Rev. Lett. **70**, 343 (1993).